ISSN (Print) 2313-4410, ISSN (Online) 2313-4402

http://asrjetsjournal.org/

An Empirical Mode Decomposition Approach for Multiple Broken Rotor Bars Detection in Three-Phase Induction Motors at No-Load Condition

Cleber Gustavo Dias[a]*, Luiz Carlos da Silva[b]

[a,b]*Informatics and Knowledge Management Graduate Program (PPGI), Nove de Julho University – UNINOVE, Rua Vergueiro 235/249, 01504-001, São Paulo, Brazil*

[a]*Email: diascg@uni9.pro.br*

[b]*Email: lumaleo1965@gmail.com*

Abstract

This paper presents an empirical mode decomposition (EMD) approach for multiple broken rotor bars detection in squirrel cage induction motors running at no-load condition, using the resultant magnetic flux density measured by a Hall Effect sensor installed between two stator slots of the electrical machine. Usually, the traditional motor current signature analysis (MCSA) has produced many cases of false indications related to, among other reasons, incorrect speed estimation, operation at low load (low slip) and nonadjacent broken bars. This study has investigated the application of the EMD technique in the signal collected from the Hall sensor, in order to detect broken rotor bars for an induction motor running at very low slip and subjected to adjacent and nonadjacent broken bars. The present approach has been validated from some experiments carried out by a 7.5 kW induction motor fed by a sinusoidal power supply in the laboratory.

Keywords: Induction Motor; Fault Diagnosis; Signal Processing.

1. Introduction

The squirrel cage induction motors (SCIMs) are rotating electrical machines widely used in the industry applications. Usually, this kind of machine is associated to a several types of drives and varying load torque conditions, being responsible for a huge amount of energy consumption around the world [1]. The SCIMs are robust equipment's when compared to other rotating machines, but they are subjected to some faults and defects in electrical or mechanical parts such as stator windings, bearings and rotor structure.

---

* Corresponding author.

Broken rotor bars are related to 10% - 20% of the total faults in SCIM and this type of failure leads to reduction of the motor life cycle, temperature rise and mechanical vibrations [2]. Over the last 20+ years the motor current signature analysis (MCSA) method has been applied for detecting broken rotor bars in squirrel cage induction motors, using rotor fault frequency sidebands as a fault index [3]. However, although this technique has been successful in this field, several works have shown some drawbacks, particularly false indications related to the operation of the SCIM at low load condition and due to nonadjacent broken bars. Other researchers [4,5] have shown that in case of bars fractured at 90º electrical, no significant variation has observed in the sideband frequencies using MCSA also leading to a false negative indications. Moreover, other works have investigated new approaches for broken rotor bars detection in case of nonadjacent broken rotor bars [6-9], including SCIM running at very low slip conditions. In [8], for example, the authors have combined the use of sideband components in the internal and external flux measurements during steady state and transitory conditions. Therefore, this work has considered the evaluation of both external stray flux and internal radial airgap flux. It should be mentioned that, the authors have applied frequency domain methods to extract sideband components as an index fault, which usually has a higher computational cost when compared to some time domain techniques. In [9], the authors has also investigated non-adjacent broken bar cases, but it is necessary looking the differences (spectrum analysis) between an actual sample and a reference signal to perform rotor fault detection. In this sense, the Empirical Mode Decomposition (EMD) and its variations have shown a good potential to detect broken rotor bars for different load torque scenarios [11-16]. In [13], for example, the authors have used EMD of stator current to detect broken bars at ¾ and ½ load torque conditions. This work did not evaluate the SCIM running at low load conditions or considering nonadjacent rotor fault cases. In [14], the authors have implemented complete ensemble empirical mode decomposition (CEEMD) in field programmable gate array (FPGA), in order to monitor broken bars in induction motors, but this work also did not address nonadjacent fault cases. Some researchers have shown the great potential of external or internal magnetic flux analysis, in order to evaluate broken rotor faults [17-21]. For large induction machines, for example, the use of a Hall Effect sensor installed near the air gap has been demonstrated good results and a great potential for broken rotor bars detection. Based on the aforementioned, this paper proposes an EMD approach for multiple broken rotor bars detection in SCIM at no-load condition, using as a fault index only the number of zero crossings of the intrinsic mode functions extracted from each operational condition. The EMD method has been applied in the signal sampled from a Hall Effect sensor installed between two stator slots of the machine. The experimental results have shown a good performance for rotor fault detection, particularly at no-load condition and considering nonadjacent cases that usually leads to false indications using MCSA method.

2. The Fundamentals of the Empirical Mode Decomposition

As cited by [1,2], the empirical mode decomposition (EMD) is a processing method proposed for analyzing a complex, stationary or nonstationary signal. In this sense, EMD performs a decomposition of the original signal into a finite series of simpler data sets called intrinsic mode functions (IMFs). As also described by [1], the extrema of the original signal $x(t)$ must be identified and the local maxima is then interpolated by a cubic spline as the upper envelope. Thus, the same calculus is carried out with the local minima to produce the lower envelope. In the next step, we should designate the mean of the upper and lower envelopes called as m_1 and then we have to calculate the difference h1 between the original signal $x(t)$ and m_1, being this value the first

component as shown by equation 1.

$$h_1 = x(t) - m_1 \quad (1)$$

In the next step, we should verify if h_1 satisfies the conditions of the IMF or a criterion to define an IMF, in order to take it as the first IMF (IMF1) of $x(t)$. Those conditions, as cited by [2], are related to the fact that in the whole dataset, the number of extrema and zero crossings (ZCs) must be the same or should differ at most by one, and at any point, the mean value of local maxima and local minima envelopes is zero. A new IMF is calculated by repeating the whole procedure dealing with residue of the original signal as a new signal. In the present study, the IMF1, IMF2, IMF3, IMF4, IMF5 and IMF6 have been calculated for the signal sampled by a Hall sensor installed two stator slots of the SCIM.

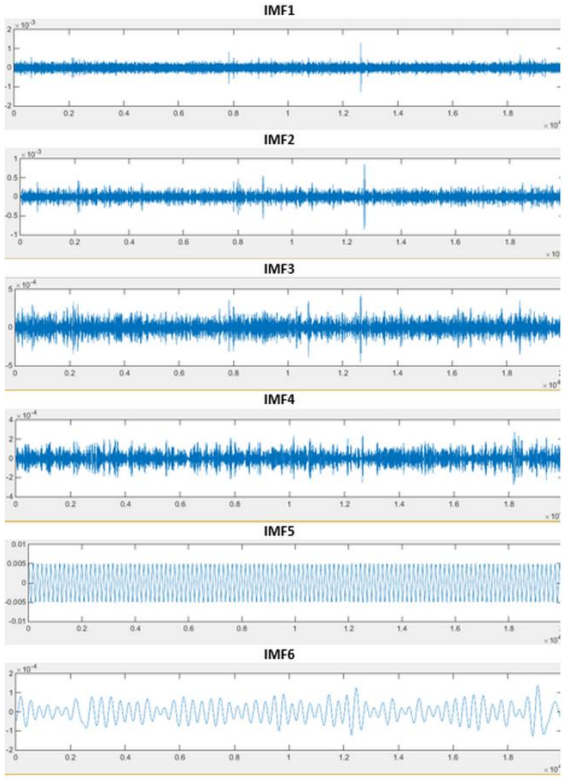

Figure 1: EMD of Hall Effect signal of an induction motor

3. Materials and Methods

In this section, we describe the experimental setup and the methodology applied for broken rotor bars detection using EMD approach for distinct operational scenarios.

3.1. Methodology

The present methodology is shown in Figure 2. It is possible to note the Hall Effect sensor installed inside the machine. The air gap magnetic flux density is measured and in case of broken rotor bars the disturbances are evaluated applying the EMD method. It should be noted that the signal obtained from the Hall sensor is a

sinusoidal waveform and rotor faults are associated to some distortions in the peak value, such as cited by other studies [15-17]. After the signal sample process, EMD has been carried out, using Matlab© software to extract IMFs components and evaluate the number of ZCs. The differences between the number of ZCs is used as an index fault for different rotor fault conditions, such as a health motor and an electrical machine with adjacent and nonadjacent broken rotor bars. In the present case, the induction motor has been fed by a sinusoidal supply and at no-load torque.

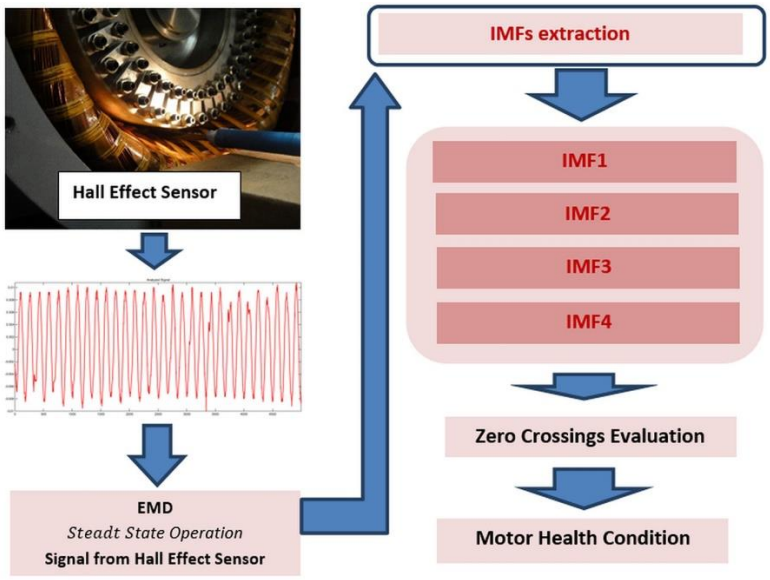

Figure 2: Proposed Methodology

3.2. Experimental Setup

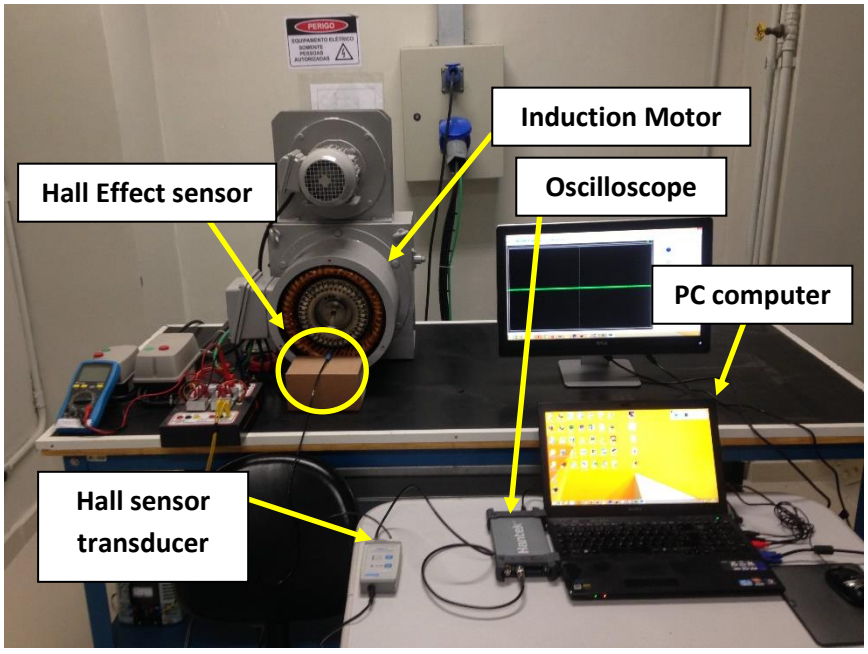

Figure 3: Experimental setup

The experimental tests have been carried out in a laboratory using an induction motor particularly manufactured for rotor fault studies. Figure 3 shows the main resources used for running each operational condition. The tests have been performed on a 7.5 kW, four pole and three-phase induction motor with a rotor cage made with 38 rotor bars. This rotor allows the user to connect the rotor bars easily to the end-ring through bolts and nuts. The signal sampled from the Hall sensor was collected using a PC computer and a USB Digital Oscilloscope (Hantek – model HT6022BE). This equipment has a bandwith in 20 MHz and maximum real-time sample rate at 48 MS/s. It should be mentioned that the Hall Effect sensor has been connected to a Hall transducer with a conversion rate at 1T/V or 0.1T/V and as cited before Hall sensor was installed inside the machine and between two stator slots.

It is important to also mention that the SCIM has an internal braking system (Foucault brake) capable of applying different mechanical loads to the motor shaft using a DC power supply.

4. Experimental Results and Discussion

For experimental evaluation purposes, the present research has carried out distinct tests using SCIM running at several operational conditions. The following subsections show the use of the present method for the induction motor running from healthy up to different damaged cases. For each scenario, the EMD method was performed using a time window of 4 s and total samples of 40.000 from the Hall sensor signal. In the present study, two index faults have been evaluated, such as the arithmetical sum of IMF2 and IMF3 components and the sum of IMF3 and IMF4. In [13], for example, the authors applied IMF2 + IMF3 for stator current transitory analysis and IMF3 + IMF4 for current steady state evaluation. It should be noted that in [13] the authors have tested the induction motor running at ¾ and ½ load, thus, not considering low load operation. In the present method, the authors have tested the index fault for the SCIM running particularly at no load condition, although other load conditions have been also performed. In the next subsection, the number of zero crossings using IMF3+IMF4 has been evaluated as a fault index for broken rotor bars detection.

4.1. Number of Zero Crossings using IMF3+IMF4 as fault index

The first experimental setup has been carried out considering a healthy motor and rotor with adjacent broken bars. The induction motor has been tested for low load conditions. The rated slip of the SCIM is 3.4%. As shown in Table 1, the number of zero crossing has demonstrated a clearly difference between a healthy rotor and one with broken rotor bars. However, in this case it should more complicated to distinguish between one broken bar (1BB) and more than one (2BB and 4BB). In addition, we have performed the same analysis for broken rotor bars separated by 90º (bars numbered as 1 and 11). As cited by other works [4, 5], Fig. 4a shows that it is not possible to detect this damaged condition using the traditional method MCSA at low slip (slip = 1%), since the left sideband frequency is canceled out. In this case, the sideband frequencies (left and right components) are only apparent for a higher load torque (slip of 2.55%), as shown in Fig. 4b.

Table 1: Number of Zero Crossings using IMF3+IMF4

Index Fault	Healthy rotor	1BB	2BB	4BB
IMF3+IMF4 (no-load)	2556	2006	1903	1980
IMF3+IMF4 (slip of 1%)	2719	2491	2352	2409
IMF3+IMF4 (slip of 1.88%)	2996	2122	2176	2566

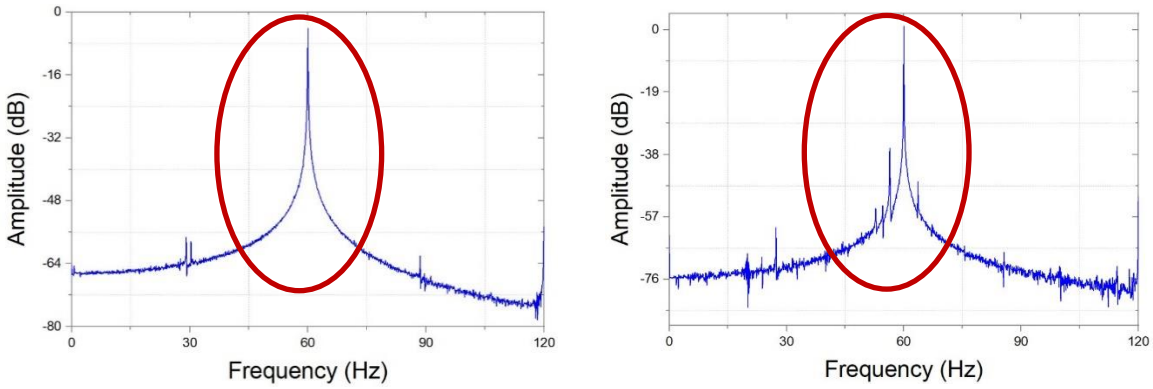

(a) (b)

Figure 4: MCSA for SCIM with two non-consecutive broken bars (1 and 11) a) motor running at slip of 1% and b) motor running at slip of 2.55%

This research has also evaluated the use of EMD method to extract the zero crossings number for SCIM running at no-load condition and for a time window of 1 s (10000 samples). Table 2 shows the values found in five experiments (Exp1 to Exp5), being possible to note the differences between a healthy condition and other with broken bars separated by 90º. In the next subsection, the number of zero crossings have been evaluated using IMF2 + IMF3 as an index fault for adjacent and nonadjacent broken bars.

Table 2: Number of Zero Crossings using IMF3+IMF4 for broken bars separated by 90º

Index Fault	Exp1	Exp2	Exp3	Exp4	Exp5	Average
IMF3+IMF4 (healthy rotor)	71	60	66	70	65	66.4
IMF3+IMF4 (broken bars 1 and 11)	50	40	43	41	45	43.8

4.2. Number of Zero Crossings using IMF2+IMF3 as fault index

In this second experimental setup, the authors have investigated the use of zero crossings of IMF2 + IMF3 for adjacent and nonadjacent broken rotor bars detection. The first dataset has been tested for Hall sensor signals sampled in a time window of 4 s (40000 samples and sample frequency = 10kHz). Table 3 shows the ZCs number for each condition and the differences between the fault index is more significant when compared to the previous case using IMF3 + IMF4, for example.

Table 3: Number of Zero Crossings using IMF2+IMF3

Index Fault	Healthy rotor	1BB	2BB	4BB
IMF2+IMF3 (no-load)	5536	5142	4983	4949
IMF2+IMF3 (slip of 1%)	5139	4872	4848	4820
IMF2+IMF3 (slip of 1.88%)	5570	5284	4982	5056

In Table 4, the number of zero crossings also shows that the application of the present approach is capable of detecting broken bars separated by 90º, even for SCIM running at no-load condition. In Fig. 5, it is possible to observe IMF2, IMF3 and IMF4 components for a healthy rotor and broken rotor bars separated by 90º.

Table 4: Number of Zero Crossings using IMF2+IMF3 for broken bars separated by 90º

Index Fault	Exp1	Exp2	Exp3	Exp4	Exp5	Average
IMF2+IMF3 (healthy rotor)	160	152	145	157	167	156.2
IMF2+IMF3 (broken bars 1 and 11)	115	96	114	100	102	105.4

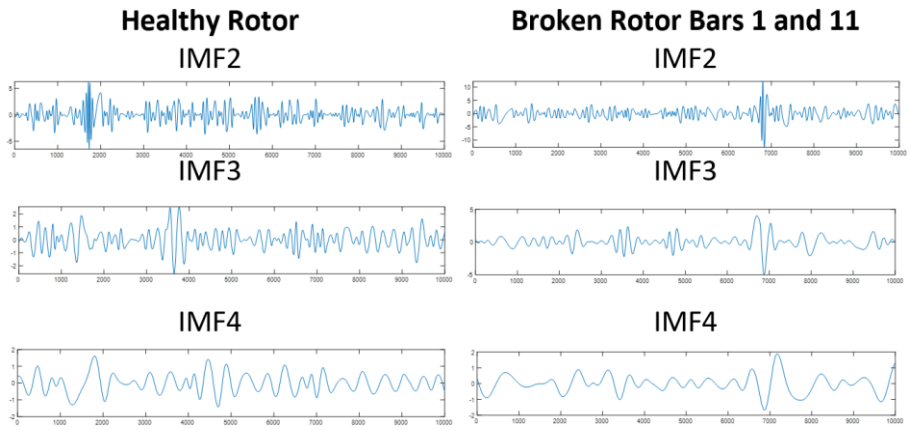

Figure 5: IMFs components for a healthy rotor and a damaged one with separated broken bars (1 and 11)

Finally, we have performed additional tests for SCIM running with nonadjacent broken rotor bars distributed for distinct magnetic poles. Fig. 6 clearly shows that the present approach is capable of identifying a healthy rotor using NZC, when compared to damaged cases. It should be mentioned that the SCIM was running at no load torque for each operational scenario.

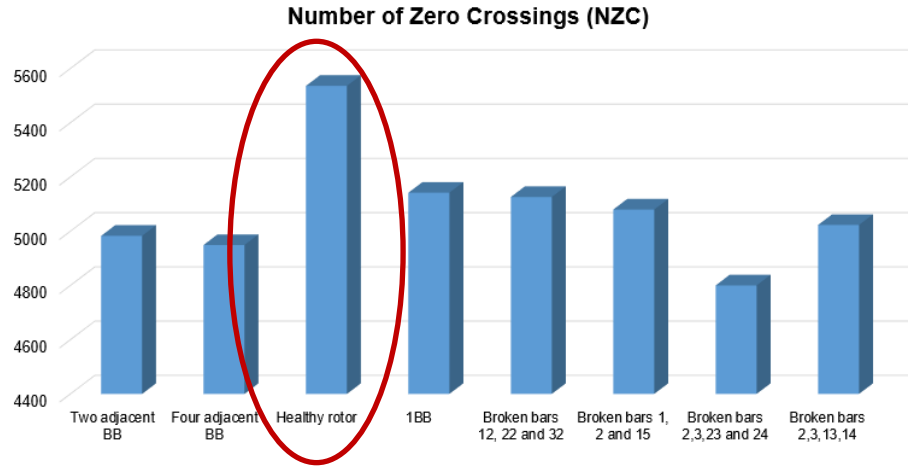

Figure 6: Number of zero crossings for different operational scenarios for motor running at no-load conditions

The present method has shown that the use of IMF2 + IMF3, or IMF3 + IMF4, as a fault index has a good potential not only to detect broken rotor bars, but also to evaluate the fault severity. More particularly, the use of IMF2+IMF3, as shown in Table 3, has highlighted that the number of zero crossings at no-load condition can be used to distinguish between a healthy motor and cases with 1BB, 2BB or 4BB. It should be noted that number of zero crossings decreases as the number of broken bars increases, for example.

5. Conclusion

This paper proposes the use of empirical mode decomposition (EMD) for multiple broken rotor bars detection, using the signal sampled from a Hall Effect sensor installed inside of the SCIM. This application is suitable for large induction motor cases, such as cited by other works [19, 21]. More particularly, the present approach has demonstrated that the number of zero crossings is able to identify a healthy rotor condition when compared to a damaged structure with broken bars. The experimental results have shown that the use of IMF2+IMF3 as a fault index provides a better rotor evaluation in view of the use of IMF3+IMF4, even for SCIM running at no-load condition and for broken bars separated by 90º electrical. Therefore, for maintenance purposes, the present study has a good performance for broken bars diagnosis considering that the SCIM could be tested under no-load condition, being possible to identify not only one broken bar but also different nonadjacent cases. It is important to mention that the present study did not address the rotor fault detection for SCIM fed by an inverter or in cases wherein the motor is subjected to oscillating loads. Finally, the authors are investigating the implementation of the present method in an embedded low cost hardware for developing an alternative tool in the future.

Acknowledgements

The authors thank the Nove de Julho University (UNINOVE) for the academic support in this research.

References

[1]. C. G. Dias, L. C. da Silva and W. A. Luz Alves, "A Histogram of Oriented Gradients Approach for Detecting Broken Bars in Squirrel-Cage Induction Motors," in IEEE Transactions on Instrumentation and Measurement, vol. 69, no. 9, pp. 6968-6981, Sept. 2020.

[2]. L. H. B. Liboni, R. A. Flauzino, I. N. da Silva, and E. C. M. Costa, "Efficient feature extraction technique for diagnosing broken bars in three-phase induction machines," Measurement, vol. 134, pp. 825–834, Feb. 2019.

[3]. S. B. Lee et al., "Identification of False Rotor Fault Indications Produced by Online MCSA for Medium-Voltage Induction Machines," in IEEE Transactions on Industry Applications, vol. 52, no. 1, pp. 729-739, Jan.-Feb. 2016.

[4]. G.Y. Sizov, A. Sayed-Ahmed, C. Yeh, N.A.O. Demerdash, "Analysis and diagnostics of adjacent and nonadjacent broken-rotor-bar faults in squirrel-cage induction machines," IEEE Trans. Ind. Electron., vol. 56, no. 11, pp. 4627-4641, Nov. 2009.

[5]. M. Riera-Guasp, et al., "Influence of nonconsecutive bar breakages in motor current signature analysis for the diagnosis of rotor faults in induction motors," IEEE Trans. Energy Convers., vol. 25, no. 1, pp. 80-89, March. 2010.

[6]. J.A. Antonino-Daviu, K.N. Gyftakis, R. Garcia-Hernandez, H. Razik, A.J.M. Cardoso, "Comparative influence of adjacent and non-adjacent broken rotor bars on the induction motor diagnosis through MCSA and ZSC methods," Proc.of IECON, pp. 1680-1685, 2015.

[7]. K. N. Gyftakis, J. A. Antonino-Daviu and A. J. M. Cardoso, "A reliable indicator to detect non-adjacent broken rotor bars severity in induction motors," Proc. of ICEM,, pp. 2910-2916, 2016.

[8]. Y. Park, H. Choi, S.B. Lee, K. Gyftakis, "Search Coil-Based Detection of Nonadjacent Rotor Bar Damage in Squirrel Cage Induction Motors", IEEE Trans. Industry Appl., vol. 56, no. 5, pp. 4748-4757, Sept-Oct. 2020.

[9]. M. E. Iglesias-Martínez, P. Fernández de Córdoba, J. A. Antonino-Daviu and J. A. Conejero, "Detection of Nonadjacent Rotor Faults in Induction Motors via Spectral Subtraction and Autocorrelation of Stray Flux Signals," in IEEE Transactions on Industry Applications, vol. 55, no. 5, pp. 4585-4594, Sept.-Oct. 2019.

[10]. Dias, C.G., de Sousa, C.M. A Neuro-Fuzzy Approach for Locating Broken Rotor Bars in Induction Motors at Very Low Slip. J Control Autom Electr Syst 29, 489–499, 2018.

[11]. Zoltowsk N. E. Huang et al., "The empirical mode decomposition and the Hilbert spectrum for nonlinear and non-stationary time series analysis," Proc. Roy. Soc. A, Math. Phys. Eng. Sci., vol. 454, no. 1971, pp. 903–995, Mar. 1988.

[12]. J. Faiz, V. Ghorbanian and B. M. Ebrahimi, "EMD-Based Analysis of Industrial Induction Motors With Broken Rotor Bars for Identification of Operating Point at Different Supply Modes," in IEEE Transactions on Industrial Informatics, vol. 10, no. 2, pp. 957-966, May 2014.

[13]. R. Valles-Novo, J. J. Rangel-Magdaleno, J. M. Ramirez-Cortes, H. Peregrina-Barreto, and R. Morales-Caporal, "Empirical mode decomposition analysis for broken-bar detection on squirrel cage induction motors," IEEE Trans. Instrum. Meas., vol. 64, no. 5, pp. 1118–1128, May 2015.

[14]. Martin Valtierra-Rodriguez, Juan Pablo Amezquita-Sanchez, Arturo Garcia-Perez, David Camarena-Martinez, "Complete Ensemble Empirical Mode Decomposition on FPGA for Condition Monitoring of Broken Bars in Induction Motors", Mathematics, vol. 7, pp. 783, 2019.

[15]. Di Liu, Xiyuan Chen, "Image denoising based on improved bidimensional empirical mode decomposition thresholding technology", Multimedia Tools and Applications, vol. 78, pp. 7381, 2019.

[16]. S. Sbaa, N. Bessous, R. Pusca and R. Romary, "A comparative study dedicated to rotor failure detection in induction motors using MCSA, DWT, and EMD techniques," 2020 International Conference on Electrical Engineering (ICEE), 2020, pp. 1-11.

[17]. A. Ceban, R. Pusca, R. Romary, "Study of rotor faults in induction motors using external magnetic field analysis," IEEE Trans. Ind. Electron., vol. 59, no. 5, pp. 2082-2093, May 2012.

[18]. G. Mirzaeva, K. I. Saad, and M. G. Jahromi, "Comprehensive diagnostics of induction motor faults based on measurement of space and time dependencies of air gap flux," IEEE Trans. Ind. Appl., vol. 53, no. 3, pp. 2657–2666, May/Jun. 2017.

[19]. Dias, C.G., Pereira, F.H. Broken Rotor Bars Detection in Induction Motors Running at Very Low Slip Using a Hall Effect Sensor. IEEE SENSORS JOURNAL, v. 18, n. 11, p. 4602-4613, Jun 2018.

[20]. J. Yun et al., "Airgap search coil-based detection of damper bar failures in salient pole synchronous motors," IEEE Trans. Ind. Appl., vol. 55, no. 4, pp. 3640-3648, July/Aug. 2019.

[21]. Dias, C.G., Da Silva, Luiz Carlos; Chabu, I.E.. Fuzzy-Based Statistical Feature Extraction for Detecting Broken Rotor Bars in Line-Fed and Inverter-Fed Induction Motors. ENERGIES, v. 12, n. 12, Jun 2019.